

SINRL: Socially Integrated Navigation with Reinforcement Learning using Spiking Neural Networks

Florian Tretter* Daniel Flögel* Alexandru Vasilache*
Max Grobbel* Jürgen Becker** Sören Hohmann**

* FZI Research Center for Information Technology,
76131 Karlsruhe, Germany (e-mail: floegel@fzi.de)

** Karlsruhe Institute of Technology, 76131 Karlsruhe, Germany
(e-mail: soeren.hohmann@kit.edu)

Abstract: Integrating autonomous mobile robots into human environments requires human-like decision-making and energy-efficient, event-based computation. Despite progress, neuromorphic methods are rarely applied to Deep Reinforcement Learning (DRL) navigation approaches due to unstable training. We address this gap with a hybrid socially integrated DRL actor-critic approach that combines Spiking Neural Networks (SNNs) in the actor with Artificial Neural Networks (ANNs) in the critic and a neuromorphic feature extractor to capture temporal crowd dynamics and human-robot interactions. Our approach enhances social navigation performance and reduces estimated energy consumption by approximately 1.69 orders of magnitude.

Keywords: human-robot interaction, intelligent human-machine interaction, social robotics and ethics, artificial intelligence in transportation, reinforcement learning and deep learning in control, task and motion planning

1. INTRODUCTION

Intelligent autonomous mobile robots are increasingly integrated in crowded environments to assist humans. Their applications range from service robots in hospitals and airports to last-mile delivery systems in urban areas. As these robots become more pervasive, recent research has begun to explore neuromorphic computing to achieve more energy-efficient systems (Xu et al., 2022), as well as biological-inspired approaches (Shim and Li, 2017) with event-based computation. Despite the progress in social navigation, two fundamental challenges remain for autonomous robots in crowded environments. First, fully leveraging the benefits of neuromorphic computing requires end-to-end architectures in which both perception and decision-making are realized on neuromorphic hardware. Second, because autonomous mobile robots navigate in human-centered environments, social navigation approaches must demonstrate socially compliant behavior to ensure safe and acceptable interactions with humans.

Social navigation is a subfield of local motion planning, focusing on solving navigation tasks in highly dynamic crowded environments. Mavrogiannis et al. (2023) divides social navigation approaches into coupled and decoupled approaches. Decoupled approaches first predict human motions and subsequently plan a collision-free trajectory, which can lead to the freezing robot problem as described by Trautman and Krause (2010). Coupled approaches consider the future crowd evolution as a joint sequential decision making and either assume a specific structure (e.g. game theoretic in Samavi et al. (2025), forces based in Helbing and Molnár (1995) or reciprocal decision making in

Optimal Reciprocal Collision Avoidance (ORCA) from van den Berg et al. (2011)), or assume insights about the principle decision making problem as in DRL approaches first proposed by Chen et al. (2017). DRL based approaches are further categorized based on the robots exhibited social behavior (Flögel et al., 2024). Social collision avoidance, with a lack of social aspects, socially aware navigation with a predefined social behavior, and socially integrated navigation, derived from sociological definitions, where the robot's social behavior is adaptive to individual human behavior and emerges through interaction.

Although recent work such as Saravanan et al. (2021) demonstrates that SNNs can improve policy search in continuous control DRL tasks, a proper hyperparameter tuning is crucial for stable training. Furthermore, research on applying SNNs to social navigation remains sparse, limited mostly to social collision avoidance with hybrid DRL ANN-SNN approaches, while socially aware or socially integrated navigation is entirely unexplored. Therefore, we propose a socially integrated hybrid DRL approach, which enables an end-to-end neuromorphic path for policy inference, resulting in improved social navigation performance and reduced energy consumption.

The main contribution of this work is a novel socially integrated hybrid DRL navigation approach that leverages the sparsity of SNNs for energy reductions and event-based computation of human-robot interactions. We first design a hybrid actor-critic DRL architecture with SNNs in the actor and the training stability of hyperparameter-insensitive ANNs in the critic network. Subsequently, a neuromorphic feature extractor with an inherent temporal

dimension is used to cope with observing a variable number of surrounding agents and capture event-based crowd-robot interactions. Finally, we benchmark our approach against state-of-the-art socially integrated and socially aware navigation approaches, and compare the estimated energy consumption of the trained models on various conventional and neuromorphic hardware platforms.

2. PRELIMINARIES

A dynamic object in the environment is generally referred to as an agent, whether it is a robot or a human, and a policy determines its behavior. Variables referring to the robot are indexed with \square^0 , and humans with \square^i , where $i \in 1, \dots, N-1$. A scalar value is denoted by \square , a vector \square is bold, and a matrix is capital bold.

2.1 Problem Formulation

The navigation task of one robot toward a goal in an environment with $N-1$ humans is a sequential decision-making problem that can be modeled as an Partially Observable Markov Decision Process (POMDP) and solved with a DRL framework (Chen et al., 2017). The POMDP is described with a 8-tuple $(\mathcal{S}, \mathcal{A}, \mathcal{T}, \mathcal{O}, \Omega, \mathcal{T}_0, R, \gamma)$. We assume the state space $\mathcal{S} \in \mathbb{R}$ and action space $\mathcal{A} \in \mathbb{R}$ as continuous. The transition function $\mathcal{T} : \mathcal{S} \times \mathcal{A} \times \mathcal{S} \rightarrow [0, 1]$ describes the probability transitioning from state $\mathbf{s}_t \in \mathcal{S}$ to state $\mathbf{s}_{t+1} \in \mathcal{S}$ for the given action $\mathbf{a}_t \in \mathcal{A}$. With each transition, an observation $\mathbf{o}_t \in \mathcal{O}$ and a reward $R : \mathcal{S} \times \mathcal{A} \rightarrow \mathbb{R}$ is returned by the environment. The observation \mathbf{o}_t is returned with probability $\Omega(\mathbf{o}_t|\mathbf{s}_t)$ depending on the sensors. The initial state distribution is denoted by \mathcal{T}_0 and $\gamma \in [0, 1]$ is the discount factor. We assume circular shaped agents and each agent, robot and humans, is completely described with a state $\mathbf{s}_t^i = [\mathbf{s}_t^{i,o}, \mathbf{s}_t^{i,h}]$ with $i \in 0, \dots, N-1$ at any given time t . The observable part $\mathbf{s}_t^{i,o} = [\mathbf{p}, \mathbf{v}, r]$ is composed of position \mathbf{p} , velocity \mathbf{v} , and radius r . The unobservable, hidden part, $\mathbf{s}_t^{i,h} = [\mathbf{p}_g, v_{\text{pref}}, \psi_{\text{pref}}, r_{\text{prox}}]$ is composed of goal position \mathbf{p}_g , preferred velocity v_{pref} , preferred orientation ψ_{pref} , and a proxemic radius r_{prox} according to the proxemic theory of Hall (1996). The world state $\mathbf{s}_t = [\mathbf{s}_t^0, \dots, \mathbf{s}_t^{N-1}]$ represents the environment at time t . One episode's trajectory τ is the sequence of states, observations, actions, and rewards over the time interval $t \in [0, T]$. The return of one episode $\mathcal{R}(\tau) = \sum_{t=0}^T \gamma^t R_t$ is the accumulated and discounted reward R_t , and the central objective is to learn the optimal robot policy π^* which maximizes the expected return:

$$\mathcal{T}(\tau|\pi) = \mathcal{T}_0 \prod_{t=0}^T \mathcal{T}(\mathbf{s}_{t+1}|\mathbf{s}_t, \mathbf{a}_t) \pi(\mathbf{a}_t|\mathbf{o}_t) \Omega(\mathbf{o}_t|\mathbf{s}_t), \quad (1)$$

$$\mathbb{E}_{\tau \sim \pi} [\mathcal{R}(\tau)] = \int_{\tau} \mathcal{T}(\tau|\pi) \mathcal{R}(\tau), \quad (2)$$

$$\pi^*(\mathbf{a}|\mathbf{o}) = \arg \max_{\pi} \mathbb{E}_{\tau \sim \pi} [\mathcal{R}(\tau)]. \quad (3)$$

Considering a stochastic environment, $\mathcal{T}(\tau|\pi)$ is the probability of a trajectory τ starting in \mathbf{s}_0 with \mathcal{T}_0 .

2.2 Spiking Neural Networks

SNNs represent the third generation of neural networks and are biologically inspired (Shim and Li, 2017). The

key difference to ANNs is the introduction of a temporal dimension within the single neuron dynamics. The communication of the neurons relies on binary or graded spikes, which are summed up in the dendrite of each neuron. The neuron then processes the accumulated spikes according to its neuron dynamics and sends out spikes. Numerous neuron models exist, each with distinct dynamics that emphasize biological plausibility, such as the Izhikevich neuron (Izhikevich, 2001), computational efficiency, as seen in the Leaky Integrate and Fire (LIF) neuron, or sparsity, as in the Sigma-Delta (SD) neuron. In this work, we investigate the Current Based (CUBA) and SD neuron model.

The CUBA neuron implements a current-based integration mechanism and is a computationally efficient simplified version of the LIF. The membrane potential $V(t)$ evolves according to

$$\tau_m \frac{dV(t)}{dt} = -(V(t) - E_L) + R_m I_{\text{syn}}(t), \quad (4)$$

with membrane time constant τ_m , resting potential E_L , and total synaptic input current $I_{\text{syn}}(t)$. A spike is emitted when $V(t)$ exceeds a threshold V_{th} , followed by a reset. This formulation assumes current-based synaptic transmission independent of the membrane potential, resulting in linear and additive input dynamics. The reduced computational complexity of the CUBA model makes it well-suited for reinforcement learning and control applications requiring efficient large-scale spiking architectures.

In contrast, the SD neuron encodes information as the temporal error between the input and its reconstructed output signal, following the principles of sigma-delta modulation. Its internal state $u(t)$ evolves as

$$\tau_m \frac{du(t)}{dt} = I(t) - \hat{I}(t), \quad (5)$$

where $I(t)$ represents the input current and $\hat{I}(t)$ denotes the reconstructed feedback current derived from emitted spikes. A spike is generated when the integrated error exceeds a threshold, and the neuron resets its internal state accordingly. This mechanism enables SD neurons to operate as adaptive, event-driven encoders with inherent temporal sparsity, allowing for efficient communication and energy usage. Compared to the CUBA neuron, the SD neuron model captures differential input dynamics, making it particularly beneficial for control tasks requiring responsiveness to rapid state changes.

3. RELATED WORK

Recent progress in energy-efficient neuromorphic hardware has sparked growing interest in applying SNNs to robotic systems, demonstrating strong potential within DRL (Jiang et al., 2023). Hybrid approaches for single-agent continuous control, such as the work by Tang et al. (2021), achieved a 140 \times reduction in power consumption on Intel's Loihi neuromorphic processor compared to an ANN baseline running on the Jetson TX2. To address POMDP scenarios, Cheng et al. (2023) extended a spiking Twin Delayed Deep Deterministic Policy Gradient (TD3) agent with an Long Short-Term Memory (LSTM)-based feature extractor, resulting in 50–80% lower deployment energy relative to ANN counterparts on PyBullet robotics benchmarks. In the context of multi-agent continuous con-

trol, Saravanan et al. (2021) reported faster training convergence and higher returns compared to ANN-based implementations. These studies highlight that neuromorphic deployment is practical and highly efficient, and current efforts are mainly focused on continuous control tasks.

Recent approaches in social navigation aim to exhibit human-like social behavior and decision-making. While state-of-the-art MPC-based approaches, such as Samavi et al. (2025), jointly optimize robots and the crowd’s motion in a bi-level structure, they rely on specific assumptions about the human motion model in the optimization problem, which do not consider social aspects, such as proxemics. In contrast, socially integrated DRL navigation approaches, as proposed by Flögel et al. (2024), do not assume a specific human motion model; they learn a navigation policy that acts according to the actions of others and treats humans individually. With this formulation, these approaches fulfill the sociological understanding of social acting and socially acceptable behavior. For a more detailed description, the reader is referred to Flögel et al. (2024) for socially integrated navigation, to Rios-Martinez et al. (2015) for proxemic theory, and to Mavrogiannis et al. (2023) for core challenges in social navigation.

In DRL social navigation architectures, a feature extractor typically precedes the actor and critic to capture crowd dynamics and handle a varying number of observed agents. In ANN-based methods, this extractor is often a Recurrent Neural Network (RNN) (e.g., an LSTM as proposed by Everett et al. (2021)) to handle an arbitrary number of agents by stacking their observations into a sequence fed to the network. The RNN accumulates information in its hidden state, producing a fixed-size feature vector used by the actor and critic. However, this sequential RNN extractor is order-sensitive, scales poorly, and fails to capture higher-order agent interactions (Chen et al., 2019).

SNN-based approaches are often employed in hybrid configurations. Tang et al. (2020) advanced this direction by jointly training spiking and non-spiking network components with their Spiking Deep Deterministic Policy Gradient (SDDPG) algorithm. When deployed on Intel’s Loihi neuromorphic processor, their method achieved higher navigation success rates and reduced energy consumption by a factor of 75 compared to baseline DRL policy on an NVIDIA Jetson TX2. Yang et al. (2023) extended this hybrid method to social collision avoidance by introducing a spiking Gated Recurrent Unit (GRU) to provide memory for multi-agent navigation. Their multi-critic architecture outperformed Tang’s SDDPG in previously unseen scenarios and produced more efficient trajectories. A related line of work was proposed by Zhang et al. (2024), who introduced Collision Avoidance Spiking Reinforcement Learning (CASRL), a hybrid framework that integrates a spiking transformer encoder with attention-based temporal fusion. Yielding improved capturing of human interaction patterns. CASRL outperformed established baselines—including ORCA, Social Aware Collision Avoidance with DRL (SA-CADRL), and SDDPG—in multi-agent settings while reducing energy consumption to 57% of the ANN counterpart.

With the promising results of hybrid DRL on social collision avoidance tasks, the research question arises whether

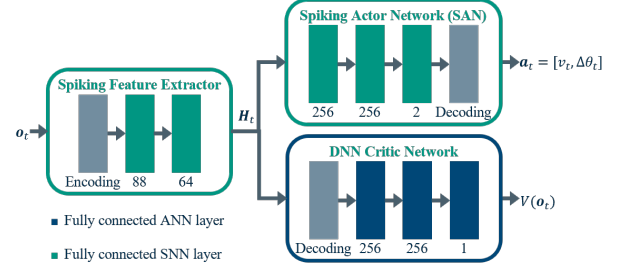


Fig. 1. Architecture composition with a temporal spiking feature output \mathbf{H}_t achieving a end-to-end spiking path.

SNN based DRL policies can capture the nuanced social dynamics of human–robot interaction for socially integrated navigation tasks while simultaneously reducing the energy consumption.

4. APPROACH

We propose a hybrid DRL framework that utilizes the Proximal Policy Optimization (PPO) algorithm (Schulman et al., 2017) with an SNN-based actor, an ANN-based critic, and a preceding Spiking Feature Extractor (SFE) as depicted in Fig. 1. The SFE leverages the inherent temporal dynamics of SNNs to more effectively capture human-robot interactions and learns an embedding of the crowd-robot interaction. This design combines the advantages of sparse and event-driven inference from the SNN for potentially lower energy consumption with the stable gradient-based learning during training from the ANN.

4.1 Hybrid Approach

We follow the framework in Flögel et al. (2024) to train a Socially Integrated (SI) navigation policy and use the same observation (Appx. A) and reward system (Appx. B). The policy is trained from scratch, respects proxemic and velocity social norms, and exhibits social behavior that is adaptive to individual human preferences. The action \mathbf{a}_t of the policy is a velocity v_t and a delta heading $\Delta\theta_t$ command. The hybrid actor-critic approach integrates a Spiking Actor Network (SAN) with a conventional ANN critic (Fig. 1). The shared SFE allows multi-agent observations by transforming the observation into a temporally encoded feature tensor. In contrast to recurrent structures that rely on artificial temporal dependencies, the SFE represents sequential dependencies through the intrinsic temporal dynamics of spiking neurons, without requiring explicit recurrent structures. The feature tensor \mathbf{H}_t serves as a direct input to the actor, whereas the critic relies on a decoder that transforms the spikes back into the floating-point domain. The critic outputs the value function $V(\mathbf{o}_t)$, evaluating the SAN and thus serving as a learning signal.

During training, the SFE, SAN, and the critic are jointly optimized using PPO. The ANN-based critic operates in the floating-point domain to ensure stable learning, while the feature extractor and actor remain in the spiking domain, enabling compatibility with neuromorphic hardware. During inference, only the spiking pathway from the SFE to the SAN is required, yielding a fully neuromorphic

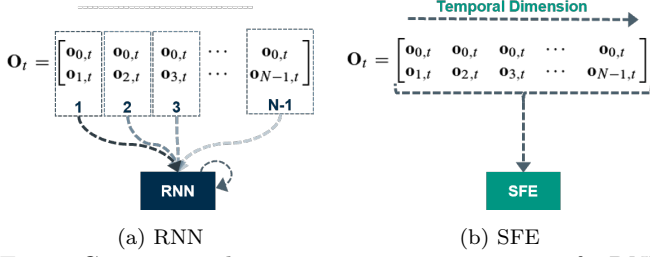


Fig. 2. Comparison between sequence processing of a RNN feature extractor approach (a) and the simplified input to our SFE approach (b).

execution pipeline from observation to action. This is particularly advantageous for deployment on neuromorphic platforms and in combination with neuromorphic perception systems. This hybrid approach decouples training efficiency from inference efficiency, allowing learning to benefit from the stability of conventional ANN training while deployment exploits the event-driven, low-power characteristics of neuromorphic computation.

4.2 Neuromorphic Encoding

To realize the neuromorphic part of the actor, conventional ANN layers are transformed into their spiking equivalents. This transformation enables the network to process information through discrete spike events rather than continuous activations, allowing temporal dynamics to emerge from the neuron model. Information transfer between the floating-point and spiking domains requires an encoding and decoding mechanism. We employ current injection as the encoding scheme, where each floating-point input value is interpreted as a synaptic input current. This allows for the direct injection of continuous observations without expanding the temporal dimension for neuron size. The neuron’s membrane potential accumulates this input over time, producing a spike train that represents the encoded signal. For decoding, the mean firing rate or the average membrane potential across the temporal dimension is used to recover a continuous representation.

Utilizing a feature extractor before the actor and critic networks enables the use of multi-agent observations and addresses the incompatibility between variable-sized input vectors and the fixed-size input layers of neural networks. The proposed SFE differs from ANN approaches in how the information is processed. We leverage the inherent temporal dimension of SNNs and do not rely on an artificial temporal dimension as in RNNs. Given an arbitrarily long input sequence \mathbf{o}_t , an RNN produces a feature vector \mathbf{h}_t that represents a weighted combination of the observations in the sequence. Contrary, neuromorphic SNN-based approaches introduce an additional inherent temporal dimension. With our proposed SFE (Fig. 2b), we use this additional temporal dimension by inserting the complete observation matrix \mathbf{o}_t with the agents stacked in the temporal dimension with:

$$\mathbf{o}_t^{H \times T} = \begin{bmatrix} \mathbf{o}_{0,t} & \mathbf{o}_{0,t} & \cdots & \mathbf{o}_{0,t} \\ \mathbf{o}_{1,t} & \mathbf{o}_{2,t} & \cdots & \mathbf{o}_{N-1,t} \end{bmatrix}. \quad (6)$$

with the robot observation $\mathbf{o}_{0,t}$ and the human observation $\mathbf{o}_{i,t}$ at time step t . For a detailed description of the observation, refer to (Appx. A). The human agents are ordered from closest to farthest away $\mathbf{o}_{N-1,t}$. By stacking the

Table 1. Assumed Energy (J) per Operation

Device	Synop Energy	Neurop Energy	Source
CPU x86	8.60×10^{-9}	8.60×10^{-9}	Degnan et al. (2016)
CPU ARM	9.00×10^{-10}	9.00×10^{-10}	Degnan et al. (2016)
GPU	3.00×10^{-10}	3.00×10^{-10}	Degnan et al. (2016)
SpiNNaker	1.33×10^{-8}	2.60×10^{-8}	Hoppner and et. al (2019)
SpiNNaker 2	4.50×10^{-10}	2.19×10^{-9}	Hoppner and et. al (2019)
Loihi	2.71×10^{-11}	8.10×10^{-11}	Davies and et. al. (2018)

robots in the temporal dimension of the SNN, we achieve a fixed-sized input H while allowing the observation of an arbitrary number of agents. Using the inherent temporal dimension, we simplified the input for the feature extractor from inserting a sequence of agents to a single matrix. Additionally, unlike the RNN feature extractor, a compression of the output to a feature vector \mathbf{h}_t can be avoided for the actor network, as our approach utilizes a SAN that also features a temporal dimension. This allows outputting the extracted features as a temporally dependent matrix \mathbf{H}_t . With the smaller compression of information, we expect a performance increase in navigation and social compliance.

The observation matrix is additionally sorted so that the closest robot has the highest influence on the output of the SFE. We invert the sequence order from Everett et al. (2021) for our concept, because of the different working principle of an SFE compared to an RNN. The first time bin of the input of a SFE enters the neuron model with its dynamics and gets outputted at the second time bin. With the second time bin of the input now entering the neuron dynamic, the information from the first input time bin remains encoded into the neuron dynamic. Therefore, the output of the third-time bin results is based on the information from the first and second input time bins. This illustrates how the initial information of the sequence of an SFE influences all future inputs and, therefore, most significantly impacts the accumulated temporal output.

4.3 Energy Calculation

The calculation of the energy consumption is inspired by the Nengo framework from Bekolay et al. (2014). It estimates the energy per inference by taking synaptic operations as well as neuron updates into consideration: $E = N_{\text{synops}} \times E_{\text{synop}} + N_{\text{neuronupdates}} \times E_{\text{neuron}}$ with E_{synop} representing the energy necessary per synaptic operation, N_{synops} representing the number of synaptic operation, E_{neuron} representing the energy per neuron update, and $N_{\text{neuronupdates}}$ is the number of neuron updates and is calculated by multiplying the number of time steps per inference with the number of neurons: $N_{\text{neuronupdates}} = N_{\text{timestep}} \times N_{\text{neurons}}$. Hence, the assumption is made that each neuron is updated at every timestep. A distinction between neuromorphic and non-neuromorphic hardware is necessary for calculating the synaptic operations.

Neuromorphic hardware is event-driven, synaptic energy is only consumed if an event occurs. This results in only multiplying every neuron that spikes, represented by the spikestate $s_{t,l,n} \in [1 = \text{spiking}, 0 = \text{else}]$, for all layers l and for each time step t times the number of non-zero synaptic connections between the layers $c_{l,n}$. This formula can be described as:

$$N_{\text{synops,neuromorphic}} = \sum_{t,l,n} s_{t,l,n} \times c_{l,n} \quad (7)$$

Table 2. PPO Hyperparameters and Rewards

Hyperparameter	SD	CUBA	Reward	Value
optimizer	Adam	Adam	R_g	4
learning rate	2×10^{-4}	9×10^{-5}	R_c	4
environment steps	256	128	R_{time}	4
clip range	0.1	0.1	$R_{gd,1}$	0.1
number of epochs	4	4	$R_{gd,2}$	0.2
batch size	256	256	R_v	0.058
discount factor γ	0.99	0.99	R_{prox}	1.1

Non-neuromorphic hardware is not event-driven, the assumption is made that all the synaptic connections are computed at each timestep. Therefore, the total Synaptic Operations (SYNOPS) is calculated by multiplying the number of synaptic connections times the time steps per inference, regardless of whether they are spiking or not:

$$N_{synops, non-neuromorph} = t \times \sum_{l,n} c_{l,n} \quad (8)$$

The hardware-specific Energy per Operation value is displayed in Table 1.

5. EVALUATION

We adhere to the principles and guidelines for evaluating social navigation, assessing the algorithm’s behavior in response to dynamic obstacles within a reproducible simulation as a preliminary stage before real-world experiments (Francis and et.al., 2023). First, we compare the training and generalization performance on different scenarios for two different SNN neuron types. Subsequently, we compare the quantitative social navigation results with the socially integrated SI-PPO (Flögel et al., 2024) and the socially aware SARL (Chen et al., 2019) policies, and provide a qualitative analysis of the learned social behavior. Finally, we evaluate the estimated power consumption of our hybrid approach on neuromorphic hardware.

5.1 Experimental Setup

For training and evaluation, we utilize the microscopic social-physiological environment described in Flögel et al. (2024). All DRL policies are trained with *Stable Baselines3* (Antonin Raffin et al., 2021). For our proposed approach, the PPO hyperparameters are obtained through a hyperparameter search performed with *Optuna* (Akiba et al., 2019) and are stated in Table 2. Other key parameters include the neuron-parameter for SD SFE: $V_{th} = 0.14$, $\tau_{grad} = 0.82$, $s_{grad} = 0.16$; the SD SAN: $V_{th} = 0.26$, $\tau_{grad} = 0.44$, $s_{grad} = 0.58$; the CUBA SFE: $V_{th} = 0.31$, $\alpha_I = 0.77$, $\alpha_V = 0.49$, $\tau_{grad} = 0.55$, $s_{grad} = 2.34$; and the CUBA SAN: $V_{th} = 0.93$, $\alpha_I = 0.16$, $\alpha_V = 0.78$, $\tau_{grad} = 0.21$, $s_{grad} = 3.47$.

To evaluate the performance and compare the different approaches, we consider three scenarios: a circle interaction scenario (8 agents), a circle crossing (8 agents), and a random scenario (10 agents). For domain randomization, start and goal locations are randomly selected within the red regions shown in Fig. 3, while the robot is randomly allocated to one of the blue start-goal pairs. In addition, the agents’ preferred speeds and the proxemic radii of humans are drawn from $\mathcal{U}[0.5, 1.0]$ and $\mathcal{U}[0.3, 0.7]$, respectively. Note that the robot cannot directly observe the proxemic radius, only implicitly through interaction behavior, since

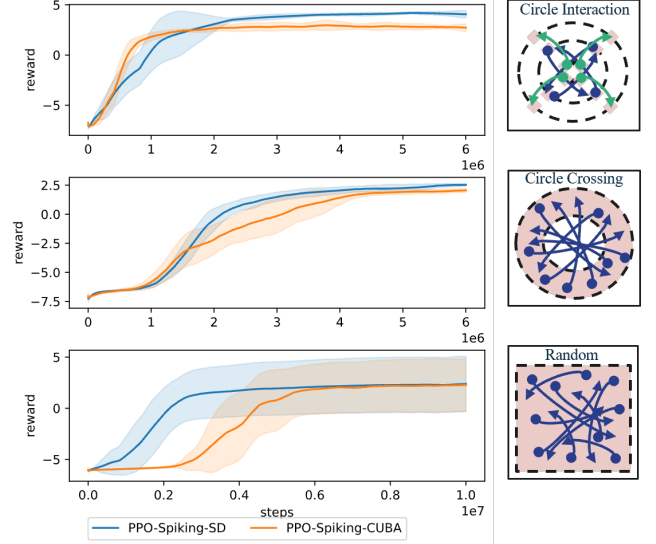


Fig. 3. Training rewards of our approach with SD and CUBA neurons across 10 seeds and different scenarios. The start and goal positions are sampled in red areas.

humans actively maintain their own proxemic radius. For further insights, refer to Flögel et al. (2024). The training on the circle interaction and circle crossing scenario is conducted over 6×10^6 steps and on the random scenario for 1×10^7 steps due to the higher complexity. To assess the generalization capability, we cross-validate the trained policies by evaluating them on the other two scenarios, thereby assessing the agent’s adaptability and the impact of the different training environments. Since the SARL baseline employs a one-step lookahead, its training and evaluation are computationally more demanding. Therefore, SARL is trained with 5 random seeds¹, whereas all other policies are trained with 10 seeds. All policies are evaluated for 200 episodes per converging seed and per scenario.

5.2 Results

Quantitative Evaluation: The training rewards in Fig. 3 illustrate stable and converging training of our hybrid method across all three scenarios for both methods. Since the circle interaction scenario has only slight randomization, the training converges the fastest. Circle crossing introduces more randomness due to the larger spawn areas for the start and goal positions, leading to later convergence. The effect is particularly pronounced when trained on the random scenario, which has the highest level of randomization. Besides the randomization regarding start and goal position, it also introduces a higher variance in the distance the agents need to travel and less interaction between agents. The proposed approach with the SD neurons achieves higher training rewards, which is especially prominent in the circle interaction and circle crossing scenario. Additionally, Spiking-PPO-SD demonstrates fast and stable training across all scenarios and seeds. Our experiments revealed that Spiking-PPO-CUBA is highly sensitive to hyperparameters, resulting in less stable and slower convergence, whereas Spiking-PPO-SD provides a robust, hyperparameter-insensitive alternative.

¹ We will provide the results across 10 seeds for the final submission

Table 3. Evaluation results with 200 episodes per scenario and seed. Goal, Collision (Col.), timeout (TO), proxemic violation (PV), distance ratio (DR): ↓

Training Scenario	Approach	Eval. Scenario: Circle Interaction					Eval. Scenario: Circle Crossing					Eval. Scenario: Random				
		Goal (%)	Col. (%)	TO (%)	PV	DR ($\mu \pm \sigma$)	Goal (%)	Col. (%)	TO (%)	PV	DR ($\mu \pm \sigma$)	Goal (%)	Col. (%)	TO (%)	PV	DR ($\mu \pm \sigma$)
Circle Interaction	SARL (Baseline)	93.00	0.00	7.00	93	1.08 ± 0.12	96.40	0.10	3.50	167	1.17 ± 1.07	52.50	1.30	46.20	191	1.67 ± 1.09
	SI-PPO (Baseline)	99.80	0.20	0.00	7	1.02 ± 0.02	93.30	4.37	2.33	169	1.06 ± 0.13	76.80	4.70	18.50	43	1.19 ± 0.40
	Spiking-PPO-SD	99.65	0.35	0.00	8	1.03 ± 0.03	88.85	2.50	8.65	83	1.05 ± 0.05	91.00	7.25	1.75	59	1.19 ± 0.49
	Spiking-PPO-CUBA	98.55	1.45	0.00	46	1.08 ± 0.08	93.05	5.95	1.00	131	1.12 ± 0.17	58.70	17.25	24.05	80	2.17 ± 4.19
Circle Crossing	SARL (Baseline)	39.90	0.4	59.70	113	2.29 ± 3.06	98.40	0.10	1.5	203	1.09 ± 0.27	31.30	1.5	67.2	218	2.26 ± 2.90
	SI-PPO (Baseline)	49.57	12.20	38.23	101	2.27 ± 2.29	86.10	7.07	6.83	52	1.74 ± 2.88	58.90	7.83	33.27	90	6.38 ± 29.49
	Spiking-PPO-SD	95.25	4.75	0.00	115	1.03 ± 0.04	99.25	0.75	0.00	27	1.03 ± 0.04	90.95	4.95	4.10	42	1.25 ± 0.67
	Spiking-PPO-CUBA	74.10	21.90	4.00	223	1.18 ± 0.29	98.30	1.70	0.00	41	1.10 ± 0.10	62.10	15.00	22.90	71	2.41 ± 8.79
Random	SARL (Baseline)	98.40	0.00	1.6	100	1.09 ± 0.10	99.40	0.10	0.50	172	1.12 ± 0.15	96.40	0.20	3.4	72	1.10 ± 0.13
	SI-PPO (Baseline)	68.03	5.60	26.37	159	2.56 ± 6.03	68.40	8.60	23.00	179	2.50 ± 5.71	80.40	2.37	17.23	66	2.40 ± 5.69
	Spiking-PPO-SD	98.35	1.60	0.05	63	1.02 ± 0.06	99.50	0.50	0.00	30	1.02 ± 0.02	88.55	4.45	7.00	40	1.27 ± 0.75
	Spiking-PPO-CUBA	88.90	3.95	7.15	111	1.28 ± 0.73	94.65	2.85	2.50	71	1.16 ± 0.42	58.50	15.90	25.60	69	2.20 ± 2.55

We consider the percentage of the robot reaching the goal, colliding with a human, the rate at which the robot runs into a timeout (TO), the number of proxemic violation (PV), and the distance ratio (DR) to evaluate the navigation performance. The DR is the fraction of traveled distance and ideal distance, which is a straight line to the goal at the preferred velocity. The evaluation results in Table 3 reveal that both proposed approaches show competitive or superior performance in all scenarios. When trained on the circle crossing scenario, the Spiking-PPO-SD outperforms both baselines and exhibits superior performance compared to the Spiking-PPO-CUBA approach. Across all scenarios, the Spiking-PPO-SD exhibits higher generalization capabilities, as evidenced by a higher success rate in non-training scenarios. Even better than the SARL baseline, which includes an imitation learning phase with ORCA expert trajectories to initialize the networks for DRL training. Across all scenarios, the socially integrated navigation policies exhibit the lowest proxemic violations, indicating an individual consideration of human interaction behavior.

Concluding the results in Table 3, the Spiking-PPO-SD demonstrates superior robustness, generalization, and adaptation to human behavior across all scenarios. It has the lowest PV and DR, indicating the highest social integration in terms of adapting to individual human behavior. Therefore, we will only further evaluate the Spiking-PPO-SD approach. We suspect that the hyperparameter sensitivity of the CUBA neurons contributes to the poorer performance, and CUBA neurons require more time steps to encode information into an information-rich spike train, thereby reducing their hyperparameter sensitivity. This also explains the superior performance of Spiking-PPO-SD, since the SD neurons can encode information at a single timestep through graded spikes.

Qualitative Evaluation: As a qualitative metric, we evaluate the robot’s trajectory and speed, as well as its interaction behavior with human agents. The ideal behavior is considerate, robust, and efficient, characterized by socially integrated navigation, which enables the robot to adapt to and coordinate with the behavior of surrounding agents, resulting in efficient navigation for all agents involved. The Spiking-PPO-SD in Fig. 4 exhibits socially integrated behavior by respecting each agent’s proxemic radius and adjusting its speed accordingly to that of surrounding agents. The robot navigates closely past the agents, adjusting its heading and slowing as needed while still following a goal-driven trajectory. Another learned behavior that shows

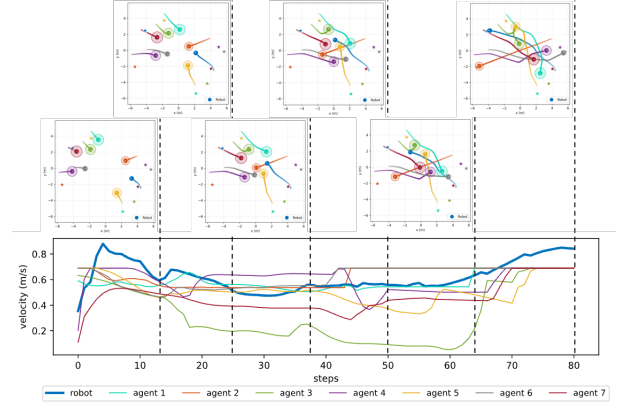


Fig. 4. Socially Integrated: The Spiking-PPO-SD policy is adaptive and respects individual human proxemics, leading to smooth trajectories for all agents.

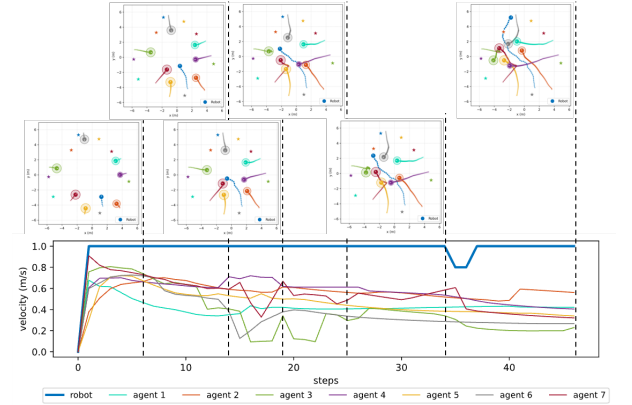


Fig. 5. Socially Aware: the SARL policy focuses on ego navigation, leading to a negative impact on human agents’ trajectories.

social integration is passing behind another agent. At step 25 in Fig. 4, the robot slows down, adjusts its heading to pass behind the second agent at step 38, and accelerates at step 64 once the social interaction is resolved. In contrast, the socially aware SARL policy in Fig. 5 mainly navigates at its maximum speed and does not adapt to human agents’ behavior. The robot reaches the center point first, but then pushes other agents away as depicted in steps 19 and 25, and violates the proxemic radius of the red agent in step 19. This leads to non-smooth trajectories of human agents in the surroundings and a negative impact on the crowd behavior. These results reveal that the ego-centric perspective of socially aware navigation

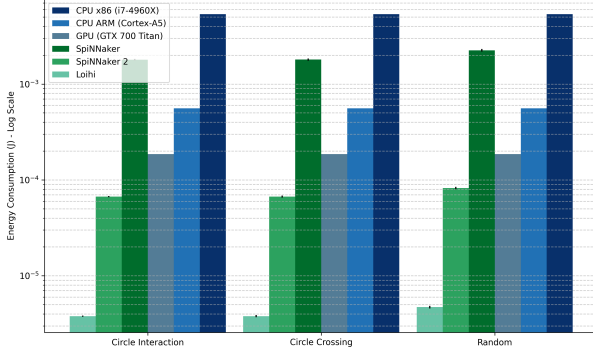


Fig. 6. Estimated energy consumption of the Spiking-PPO-SD on different hardware and scenarios.

policies may lead to goal-directed robot trajectories but has a negative impact on the behavior of other agents. In contrast, the socially integrated navigation policy with its adaptive behavior leads to goal-driven trajectories of all agents involved and even to short traveled distances as revealed through the DR in Table.3.

Energy Consumption: The estimated energy consumption of the Spiking-PPO-SD over 200 evaluation episodes across all three scenarios is displayed in Fig. 6. Since sparsity affects only the neuromorphic estimated energy consumption during synaptic updates, only the neuromorphic hardware devices vary across evaluation samples. In contrast, the conventional hardware produces the same estimated energy consumption across evaluation samples. The estimated energy consumption is the lowest for the Loihi with $3.79 \pm 0.06 \mu J$ on the circle interaction, $3.79 \pm 0.10 \mu J$ on the circle crossing, and $4.71 \pm 0.14 \mu J$ on the random scenario. The second lowest energy consumption was estimated on the SpiNNaker 2 with $66.86 \pm 1.00 \mu J$ on the circle interaction, $66.93 \pm 1.68 \mu J$ on the circle crossing, and $82.17 \pm 2.38 \mu J$ on the random scenario. The first conventional hardware is the GPU (GTX 700 Titan) with $186.33 \mu J$ followed by the ARM CPU (Cortex-A5), of $559.00 \mu J$. Finally, the SpiNNaker is estimated to consume $1.19 \pm 0.03 mJ$ on the circle interaction, $1.15 \pm 0.03 mJ$ on the circle crossing, and $1.29 \pm 0.08 mJ$ on the random scenario, while the highest estimated energy consumption was reached by the x86 CPU (i7-4960X) with $5.34 mJ$. The 1.60 – 1.69 magnitude lower estimated energy consumption obtained by running our Spiking-PPO-SD on a neuromorphic device, such as the Loihi, compared to running on conventional hardware, showcases the potential energy improvements that can be obtained through neuromorphic computing.

6. CONCLUSION

This work presents SINRL, a hybrid Deep Reinforcement Learning (DRL) approach for socially integrated navigation in pedestrian-rich environments using Spiking Neural Network (SNN). We propose a novel Spiking Feature Extractor (SFE) that enables the efficient encoding of multi-agent observations with the combination of a Spiking Actor Network (SAN), and a Artificial Neural Network (ANN) critic for stable training. The SFE efficiently encodes social-temporal interactions between the crowd and humans. Our experiments reveal that Sigma-Delta (SD)

neurons provide more stability during training and yield better results compared to CUBA neurons. The proposed navigation approach outperforms existing methods in social adaptation and navigation capabilities. In addition, the neuromorphic implementation has potentially lower energy efficiency compared to a conventional ANN approach. Future work aims to validate the potential energy benefits by deploying the trained SNNs on the Loihi 2.

REFERENCES

- Akiba, T., Sano, S., Yanase, T., Ohta, T., and Koyama, M. (2019). Optuna: A next-generation hyperparameter optimization framework. In *Intern. Conf. on Knowl. Discovery and Data Mining*, 2623–2631.
- Antonin Raffin, Ashley Hill, Adam Gleave, Anssi Kanervisto, Maximilian Ernestus, and Noah Dormann (2021). Stable-baselines3: Reliable reinforcement learning implementations. *Journal of Machine Learning Research*, 22(268), 1–8.
- Bekolay, T., Bergstra, J., Hunsberger, E., DeWolf, T., Stewart, T.C., Rasmussen, D., Choo, X., Voelker, A.R., and Eliasmith, C. (2014). Nengo: a Python tool for building large-scale functional brain models. *Frontiers in Neuroinformatics*, 7.
- Chen, C., Yuejiang Liu, Sven Kreiss, and Alexandre Alahi (2019). *Crowd-Robot Interaction: Crowd-aware Robot Navigation with Attention-based Deep Reinforcement Learning*. IEEE, Piscataway, NJ.
- Chen, Y.F., Liu, M., Everett, M., and How, J.P. (2017). Decentralized non-communicating multiagent collision avoidance with deep reinforcement learning. In *2017 IEEE International Conference on Robotics and Automation (ICRA)*, 285–292. IEEE.
- Cheng, H., Duan, F., and He, M. (2023). Spiking Memory Policy with Population-encoding for Partially Observable Markov Decision Process Problems. *Cognitive Computation*, 15(4), 1153–1166.
- Davies, M. and et. al. (2018). Loihi: A neuromorphic manycore processor with on-chip learning. *IEEE Micro*, 38(1), 82–99.
- Degnan, B., Marr, B., and Hasler, J. (2016). Assessing Trends in Performance per Watt for Signal Processing Applications. *IEEE Transactions on Very Large Scale Integration (VLSI) Systems*, 24(1), 58–66.
- Everett, M., Chen, Y.F., and How, J.P. (2021). Collision avoidance in pedestrian-rich environments with deep reinforcement learning. *IEEE Access*, 9, 10357–10377.
- Flögel, D., Fischer, L., Rudolf, T., Schürmann, T., and Hohmann, S. (2024). Socially integrated navigation: A social acting robot with deep reinforcement learning. In *2024 IEEE/RSJ International Conference on Intelligent Robots and Systems (IROS)*. IEEE.
- Francis, A. and et.al. (2023). Principles and guidelines for evaluating social robot navigation algorithms. *J. Hum.-Robot Interact.*, 14.
- Hall, E.T. (1996). *The hidden dimension*. Anchor Books, New York.
- Helbing and Molnár (1995). Social force model for pedestrian dynamics. *Physical review. E, Statistical physics, plasmas, fluids, and related interdisciplinary topics*, 51(5), 4282–4286.
- Hoppner, S. and et. al (2019). Dynamic Power Management for Neuromorphic Many-Core Systems. *IEEE*

Transactions on Circuits and Systems I: Regular Papers, 66(8), 2973–2986. Publisher: IEEE.

Izhikevich, E.M. (2001). Resonate-and-fire neurons. *Neural Networks*, 14(6), 883–894.

Jiang, J., Kong, D., Hou, K., Huang, X., Zhuang, H., and Fang, Z. (2023). Neuro-planner: A 3d visual navigation method for mav with depth camera based on neuro-morphic reinforcement learning. *IEEE Transactions on Vehicular Technology*, 72(10), 12697–12712.

Mavrogiannis, C., Baldini, F., Wang, A., Zhao, D., Trautman, P., Steinfeld, A., and Oh, J. (2023). Core challenges of social robot navigation: A survey.

Rios-Martinez, J., Spalanzani, A., and Laugier, C. (2015). From proxemics theory to socially-aware navigation: A survey. *International Journal of Social Robotics*, 7(2), 137–153.

Samavi, S., Han, J.R., Shkurti, F., and Schoellig, A.P. (2025). Siconav: Safe and interactive crowd navigation using model predictive control and bilevel optimization. *IEEE Transactions on Robotics*, 41, 801–818.

Saravanan, M., Kumar, P.S., Dey, K., Gaddamidi, S., and Kumar, A.R. (2021). Exploring spiking neural networks in single and multi-agent rl methods. In *2021 International Conference on Rebooting Computing (ICRC)*, 88–98.

Schulman, J., Wolski, F., Dhariwal, P., Radford, A., and Klimov, O. (2017). Proximal policy optimization algorithms.

Shim, M.S. and Li, P. (2017). Biologically inspired reinforcement learning for mobile robot collision avoidance. In *2017 International Joint Conference on Neural Networks (IJCNN)*, 3098–3105.

Tang, G., Kumar, N., and Michmizos, K.P. (2020). Reinforcement co-learning of deep and spiking neural networks for energy-efficient mapless navigation with neuromorphic hardware.

Tang, G., Kumar, N., Yoo, R., and Michmizos, K. (2021). Deep Reinforcement Learning with Population-Coded Spiking Neural Network for Continuous Control. In *Proceedings of the 2020 Conference on Robot Learning*, 2016–2029. PMLR. ISSN: 2640-3498.

Trautman, P. and Krause, A. (2010). Unfreezing the robot: Navigation in dense, interacting crowds. In *2010 IEEE/RSJ International Conference on Intelligent Robots and Systems*, 797–803. IEEE.

van den Berg, J., Guy, S.J., Lin, M., and Manocha, D. (2011). Reciprocal n-body collision avoidance. In B. Siciliano, O. Khatib, F. Groen, C. Pradalier, R. Siegwart, and G. Hirzinger (eds.), *Robotics Research*. Springer Berlin Heidelberg.

Xu, R., Wu, Y., Qin, X., and Zhao, P. (2022). Population-coded spiking neural network with reinforcement learning for mapless navigation. In *2022 International Conference on Cyber-Physical Social Intelligence (ICCSI)*, 518–523.

Yang, B., Yuan, M., Zhang, C., Hong, C., Pan, G., and Tang, H. (2023). Spiking Reinforcement Learning with Memory Ability for Mapless Navigation. In *2023 IEEE/RSJ International Conference on Intelligent Robots and Systems (IROS)*, 1–8.

Zhang, C., Yip, K.W., Yang, B., Zhang, Z., Yuan, M., Yan, R., and Tang, H. (2024). Casrl: Collision avoidance with spiking reinforcement learning among dynamic,

decision-making agents. In *2024 IEEE/RSJ International Conference on Intelligent Robots and Systems (IROS)*, 8031–8038.

Appendix A. OBSERVATION

We follow the proposed observation in Flögel et al. (2024). The observation is divided into the robot $\mathbf{o}_{0,t} = [d_g, \Delta, \mathbf{p}_g, \theta, v_{\text{pref}}, r_0]$ and human observation $\mathbf{o}_{i,t} = [\bar{\mathbf{o}}_i, \hat{\mathbf{o}}_{i,t}]$. Based on humans’ observable states, the robot observes the human i at time t with $\bar{\mathbf{o}}_i = [r_i, r_i + r_0]$ and $\hat{\mathbf{o}}_{i,t} = [d_t, \Delta, \mathbf{p}_t, \Delta, \mathbf{v}_t]$. The robot observes its state based on the relative position to the goal $\Delta \mathbf{p}_g = \mathbf{p}_g - \mathbf{p}_t$, the direct distance to the goal $d_g = \|\Delta \mathbf{p}_g\|_2$, the heading θ , the preferred velocity v_{pref} , and the personal radius r . We distinguish the human observation into a constant part $\bar{\mathbf{o}}_i$, which remains unchanged over time, and a time-varying part $\hat{\mathbf{o}}_{i,t}$, which varies throughout the steps. The constant part contains the human radius r_i and the combined radius $r_i + r_0$. The temporal observation $\hat{\mathbf{o}}_{i,t}$ contains the relative position $\Delta \mathbf{p}_t = \mathbf{p}_{0,t} - \mathbf{p}_{i,t}$, direct distance $d_t = \|\Delta \mathbf{p}_t\|_2$, and relative velocity $\Delta \mathbf{v}_t = \mathbf{v}_{0,t} - \mathbf{v}_{i,t}$ between robot and human. To consider the partial history, we concatenate the last k temporal observations to the aggregated observation $\mathbf{o}_{i,t}$ of human i at timestep t

$$\mathbf{o}_{i,t} = [\bar{\mathbf{o}}_{i,t} \ \hat{\mathbf{o}}_{i,t} \ \hat{\mathbf{o}}_{i,t-1} \ \cdots \ \hat{\mathbf{o}}_{i,t-k}]. \quad (\text{A.1})$$

Appendix B. REWARD SYSTEM

In the socially integrated reward formulation from Flögel et al. (2024), each agent in the environment has a reward system. Humans reward the robot based on the interaction between the human and the robot. From this principle, the robot accumulates all human rewards with

$$R_{\text{SA}} = \frac{1}{M} \sum_{i=1}^M \lambda_i R_i \quad (\text{B.1})$$

at each time step. With the reward R_i of human i , a scaling factor λ_i , and the number of humans M within the social integration radius r_{SI} around the center of the robot. If the human i is within the social integration radius of the robot $d_{0i} < r_{\text{SI}}$, the human reward is given at every time step by $R_i = -R_v \cdot |v_{i,t} - v_{0,t}| - R_{\text{prox}}$. The reward comprises velocity deviations scaled with R_v and rewards violations of humans’ personal space $d_{i0} < r_{i,\text{prox}}$ with R_{prox} . In addition, the robot is rewarded for efficient navigation with R_{Nav} , which leads to the total reward $R_t = R_{\text{Nav}} + R_{\text{SA}}$ at time step t . The navigation reward teaches efficient navigation toward the goal while avoiding collisions.

$$R_{\text{Nav}} = \begin{cases} +R_g & \text{if } \mathbf{p}_t = \mathbf{p}_g \\ -R_c & \text{if } d_{0i} \leq 0 \\ -R_{\text{time}} & \text{if timeout} \\ +R_{gd,1} \cdot |\Delta d_g| & \text{if } \Delta d_g > 0 \\ -R_{gd,2} \cdot |\Delta d_g| & \text{if } \Delta d_g < 0 \end{cases} \quad (\text{B.2})$$

The robot is encouraged to take steps toward the goal with $R_{gd,1}$, where $\Delta d_g = d_{g,t} - d_{g,t-1}$, and reach the goal with R_g . Conversely, the robot is penalized for collisions with other agents with R_c , running into timeouts with R_{time} , and taking steps away from the goal with $R_{gd,2}$.